arXiv:1703.05181v1 [cond-mat.mes-hall] 15 Mar 2017

Generation of single skyrmions by picosecond magnetic field pulses

Vegard Flovik and Alireza Qaiumzadeh*
Department of Physics, Norwegian University of Science and Technology, NO-7491 Trondheim, Norway

Ashis K. Nandy
Peter Grünberg Institut and Institute for Advanced Simulation, Forschungszentrum Jülich and JARA, D-52425 Jülich, Germany

Changhoon Heo and Theo Rasing
Radboud University, Institute for Molecules and Materials, Heyendaalseweg 135, 6525 AJ Nijmegen, The Netherlands

(Dated: March 16, 2017)

We numerically demonstrate an ultrafast and novel method to create *single* skyrmions in a *collinear* ferromagnetic sample by applying a picosecond magnetic field pulse in the presence of Dzyaloshinskii-Moriya interaction. For small samples the (effective) magnetic field pulse applied could be either spatially uniform or non-uniform while for large samples a non-uniform and localized field is more effective. We examine the phase diagram of pulse width and amplitude for the nucleation and show how a spin wave instability, via magnonic spin-orbit torques, destabilizes the uniform ground state and transforms it to a metastable skyrmionic state. Our finding could ultimately be used to design future skyrmion-based devices.

PACS numbers: 75.78.-n, 75.10.Hk, 75.70.Kw, 75.78.Cd

Skyrmions, nanoscale swirling magnetic structures, are topological solitons that might be utilized as magnetic bits in the next generation of compact memory devices [1–13], thanks to their small size and intrinsic stability. It is believed that nano-scale static skyrmions with a fixed topological number $Q = \pm 1$, are stabilized in the presence of a chiral Dzyaloshinskii-Moriya interaction (DMI), so-called DMI stablized skyrmions [1–6] while long-range dipole interaction stabilizes bubble skyrmions [14–16] with an integer topological number and much larger diameters.

The possibility of a spontaneous skyrmion ground state in chiral magnets was first predicted by Rößler *et al.* [5]. The first observation of a metastable skyrmionic state in the form of a skyrmion lattice in the chiral magnet MnSi was reported by Mühlbauer *et al.* in 2009 [17]. Since then, skyrmion lattices have been observed in various non-centrosymmetric materials and ultrathin helimagnets through different experimental techniques [17–22]. Recently, the generation of skyrmion lattices at room temperature was also demonstrated [23–25]. Moreover a skyrmion lattice was observed in a Si-wafer-based multilayer system [26], making promises for future technology more realistic.

However, for applications, the generation of an isolated skyrmion is obviously more interesting than a lattice, as individual skyrmions can be used as bits of information [8, 27, 28]. In case of a single skyrmion, the creation methods are distinct from the ones for skyrmion lattices and so far, few have been demonstrated, either numerically or experimentally. It was numerically shown that charge currents, spin-polarized currents, local heating, and spin waves can create isolated skyrmions in chiral ferromagnetic systems [29–34]. All numerical simulations so far have predicted skyrmion nucleation in nanoseconds, and e.g. in [29] a circulating current is essential whereas in [30] an unrealistic damping parameter larger than 0.1 is needed. Romming *et al.* observed the creation and annihilation of single skyrmions using a spin-polarized scanning tunneling microscope tip [35], but to nucleate them an external magnetic field as well as very low temperature was needed. On the other hand, single skyrmions stabilized by dipole interactions were observed in a ferrimagnetic thin film of TbFeCo using ultrashort single optical laser pulses [36], but those had a size of more than 100 nm.

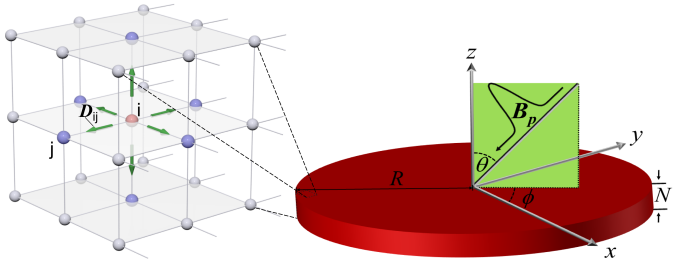

FIG. 1: (Color online) Schematic representation of the simulated system. We consider a nanodisc of radius R and thickness N atomic layers, with an underlying square lattice structure. Direction of the Gaussian magnetic field pulse is defined by the polar angle θ and azimuthal angle ϕ.

In this Letter we propose an efficient method for the nucleation of a skyrmion at a subnanosecond time scale in a uniform ferromagnetic sample using picosecond Gaussian magnetic field pulses, see Fig. 1. For a large enough

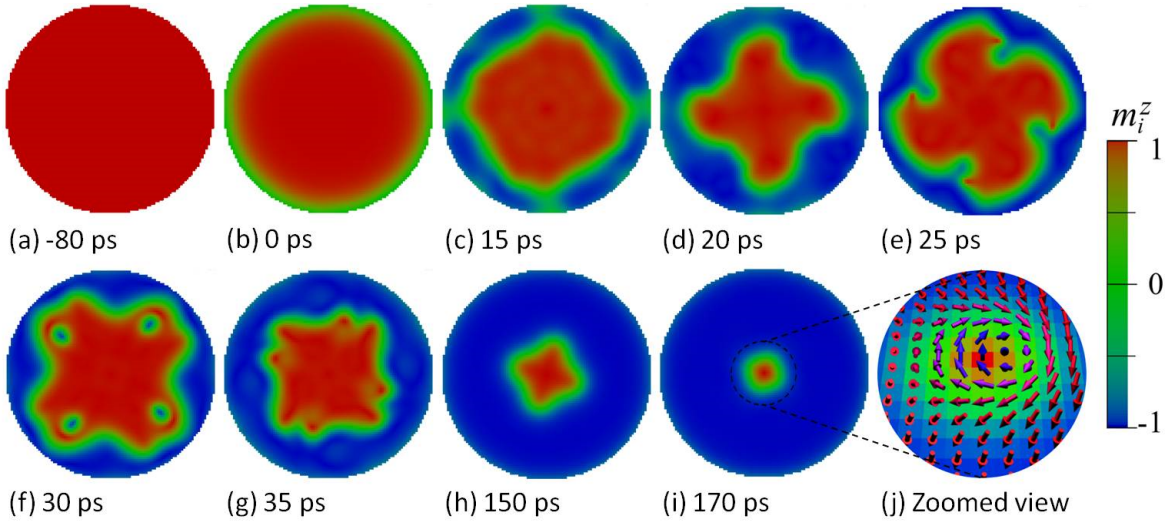

FIG. 2: (Color online) Time evolution snapshots of the magnetic spin configuration induced by a single 20 ps Gaussian magnetic field pulse normal to a circular nanodisc. (a) The initial state is a ferromagnetic state in the upward direction. (b) The maximum peak of a Gaussian magnetic field pulse arrives at $t = 0$, and a domain with inplane spin direction emerges from the edge. (c) Remaining domain in the center has circular form, while the edge area shows reversed magnetization. (d-i) After passing of the pulse the shape of the center domain gradually changes from a circular to a cross shape, as a results of interference of spin waves. (j) Ultimately one chiral Bloch type skyrmion is stablized in the center of the nanodisc.

magnetic field pulse and for certain angles, spin waves are excited in the system and destabilize the ground state by exerting a magnonic spin-orbit torque on the localized spins. Subsequently, a skyrmion is dynamically nucleated in a metastable state in the presence of DMI. Successful nucleation of a skyrmion is observed regardless of the sample geometry and size, in the presence of both spatially uniform and localized magnetic fields.

We use a classical model of localized magnetic spins. The total Hamiltonian of the system is given by,

$$\mathcal{H} = \mathcal{H}_{\rm ex} + \mathcal{H}_{\rm DMI} + \mathcal{H}_{\rm ani} + \mathcal{H}_{\rm Z}, \qquad (1)$$

where $\mathcal{H}_{\rm ex} = -J\sum_{i,j} \boldsymbol{m}_i \cdot \boldsymbol{m}_j$ is the exchange interaction between neighboring local magnetic moments $\boldsymbol{m}_i = \boldsymbol{\mu}_i/\mu_{\rm s}$, and J is the exchange constant. $\mathcal{H}_{\rm DMI} = -\sum_{i,j} \boldsymbol{D}_{ij}\cdot\boldsymbol{m}_i\times\boldsymbol{m}_j$ is the Dzyaloshinskii-Morya interaction where the DM vector $\boldsymbol{D}_{ij}$ for bulk DMI is defined as $\boldsymbol{D}_{ij} = D\boldsymbol{r}_{ij}$. For interfacial DMI $\boldsymbol{D}_{ij} = D(\hat{z}\times\boldsymbol{r}_{ij})$, with D the strength of DMI, $\boldsymbol{r}_{ij}$ a unit vector pointing from site i to site j, and $\hat{z}$ is the inversion symmetry breaking direction. $\mathcal{H}_{\rm ani} = -K\sum_i (m_i^z)^2$ is the anisotropy energy and K is the out-of-plane uniaxial anisotropy constant. The coupling of applied external magnetic field $\boldsymbol{B}_{\rm p}$ and the local spins is described by the Zeeman interaction $\mathcal{H}_{\rm Z} = -\mu_{\rm s}\sum_i \boldsymbol{m}_i \cdot \boldsymbol{B}_{\rm p}$. Here we assume $\mu_{\rm s} = 2\mu_{\rm B}$, where $\mu_{\rm B}$ is the Bohr magneton. In our simulations we consider a thin film of three layers of magnetic atoms assuming a simple cubic lattice structure with lattice constant a, see Fig. 1. Our simulations show that, within the considered geometries, the effect of dipole interaction on the skyrmion nucleation is negligible, thus we ignore that. In our simulations we assume a DMI strength less than the critical value $D < D_c = 2\sqrt{JK}$, thus the ground state is collinear [37]. The spin dynamics is described by the Landau-Lifschitz-Gilbert equation [38],

$$\frac{d\boldsymbol{m}_i}{dt} = \frac{1}{1+\alpha^2}\boldsymbol{m}_i \times (\frac{\partial\mathcal{H}}{\partial\boldsymbol{m}_i} + \alpha\boldsymbol{m}_i \times \frac{\partial\mathcal{H}}{\partial\boldsymbol{m}_i}), \qquad (2)$$

where α is the dimensionless Gilbert damping coefficient. We have utilized a time dependent magnetic field pulse defined by a Gaussian function, $\boldsymbol{B}_{\rm p}(t) = B_0(\boldsymbol{r})\exp(-\frac{t^2}{2t_{\rm w}^2})\hat{e}_{\rm B}$ applied in a direction $\hat{e}_{\rm B}$. $B_0(\boldsymbol{r})$ and $t_{\rm w}$ are the amplitude and the Gaussian width of the pulse, respectively. In experiments, however, the full width at half maximum (FWHM) of the peak is often used and is given by FWHM $= 2t_{\rm w}\sqrt{2\ln 2} \sim 2.35t_{\rm w}$. $B_0(\boldsymbol{r})$ can be either uniform through the whole sample or localized with a Gaussian profile inside the domain.

To describe the topological properties we follow the Berg and Lüscher definition of topological charge on a discrete lattice [40], $Q = \frac{1}{4\pi}\sum_l A_l$, where A_l is the area of the spherical triangle with vertices $\boldsymbol{m}_1$, $\boldsymbol{m}_2$, and $\boldsymbol{m}_3$, and the summation runs over all elementary triangles l, defined on the square lattice. The area can be calculated via $\cos(A_l/2) = \big(1 + \sum_{m<n}\boldsymbol{m}_m \cdot \boldsymbol{m}_n\big)/\sqrt{2\Pi_{m<n}(1+\boldsymbol{m}_m\cdot\boldsymbol{m}_n)}$, where $m, n = \{1,2,3\}$. The sign of A_l is determined as $\text{sign}[A_l] = \text{sign}[\boldsymbol{m}_1 \cdot (\boldsymbol{m}_2\times\boldsymbol{m}_3)]$. The topological charge of a single skyrmion is $Q = \pm 1$.

We used an atomistic classical spin dynamics simulation method implemented in the juSpinX code [41] to study the temporal evolution of the magnetization. We

also checked the results for larger samples, and investigated the effects of having a spatially localized field pulse by performing micromagnetic simulations using the simulation package MuMax3 [39].

In our atomistic simulations we consider a nanodisc of $100a \times 3a$, where a is the lattice constant, and the time step is 1 fs. A typical simulation time is about 1 ns, which is long enough compared to a typical pulse width, t_{w}, of the order of tens of ps. The magnetic field is uniform and covers the entire sample. The used material parameters for atomistic spin dynamics are the exchange stiffness J = 5 meV/atom and dimensionless parameters K/J = 0.1, D/J=0.16 and $\alpha = 0.05$. For micromagnetic simulations we assumed a nanodisc of 500 nm in diameter with material parameters for CoPt and FeGe thin films, see Supplemental Material [48].

Fig. 2 shows snapshot images of the temporal evolution of the magnetization in the nanodisc sample. The magnetic field pulse is applied at normal direction with an amplitude $B_0 = 3.5$ T and a pulse width $t_{\mathrm{w}} = 20$ ps. We found similar dynamics in a rectangular geometry in the atomistic simulation. Also the micromagnetic simulations for large nanodisc sizes and applying tilted magnetic fields show similar temporal evaluation, see Supplemental Material [48].

When the peak of the incident pulse arrives at $t = 0$, the sample becomes destabilized due to the excitation of spin waves and consequently magnonic spin orbit torque exerted on the local spins [42]. While all localized spins are collinear within the sample, at the edges the combination of DMI and finite size effect causes a tilting of the spin directions. Applying a uniform and perpendicular magnetic field pulse then excites spin waves at the edges. For the nucleation of a skyrmion, the amplitude of the pulse must be large enough to destabilize the uniform ferromagnetic state. The pulse amplitude turns completely off at about 40 ps. As the final outcome, a chiral vortex-like skyrmion in the center becomes stabilized with the topological charge $Q = +1$. The time to nucleate a skyrmion in this way is of the order of 200 ps and is much faster than in other proposed methods using currents and current pulses [30, 32]. The formation of a domain with four fold symmetry in the center of the sample during the nucleation process, Fig. 2 (c-h), originates from the symmetry of the underlying lattice structure, i.e. the square lattice.

The total energy of the system E_{tot}, is the sum of the exchange energy E_{ex}, the DMI energy E_{DMI}, the anisotropy energy E_{ani}, and the Zeeman energy E_{Z}, Eq. (1). Figs. 3 (a) and 3 (b) show the temporal evolution of each energy contribution resulting from the Gaussian magnetic field pulse B_p. The separation into two figures is necessary due to the huge difference in energy scales between the exchange energy and the rest. Compared to the initial ferromagnetic state, the newly formed skyrmionic state is a metastable state with slightly higher total energy, but the DMI energy becomes lower. The changing energies due to B_p are accompanied by a changing Q and, when all energies are stabilized at about 40 ps, Q has eventually stabilized to one, Fig. 3(c).

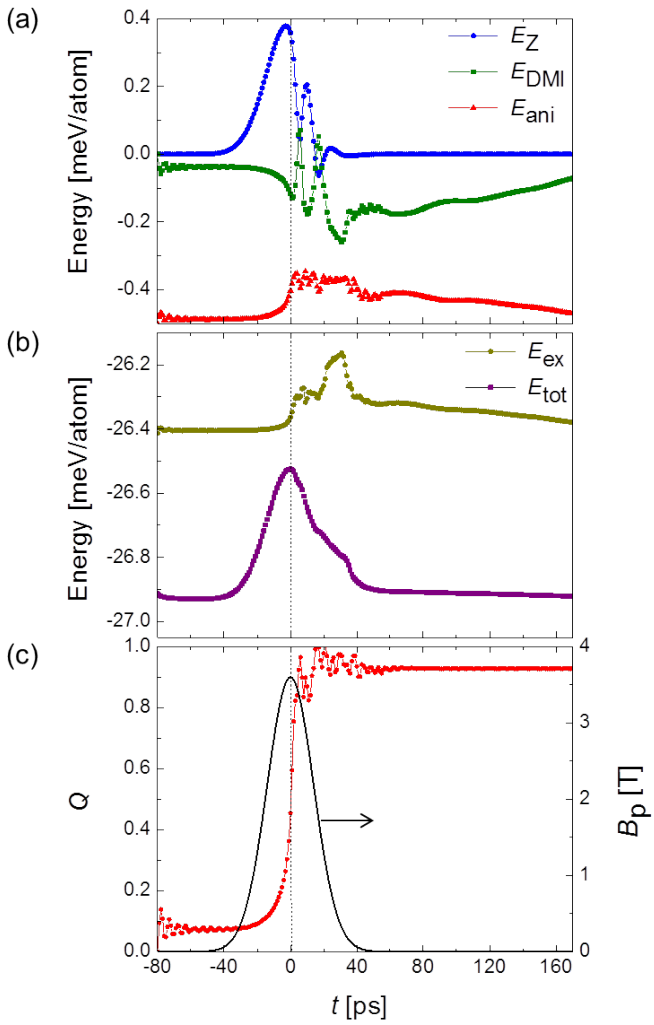

FIG. 3: (Color online) Time dependent energy contributions and topological charge Q, in a circular nanodisc during a spatially uniform magnetic field pulse with 3.5 T amplitude and 20 ps pulse width. (a) The Zeeman energy (blue dotted line) varies together with the changing of the magnetic field pulse until the pulse has completely passed the system around 50 ps. The green line indicates the variation of the DMI energy. The red line shows the change of the anisotropy energy. (b) Temporal evolution of the exchange energy and the total energy. (c) Q changes from $Q = 0$ to $Q = +1$ as the maximum peak of the Gaussian magnetic field pulse arrives at the system (vertical dashed line). Black line indicates the Gaussian magnetic field pulse.

In Fig. 4 the phase diagrams of the nucleation of a skyrmion for both atomistic and micromagnetic simulations are shown. With the parameters chosen for the atomistic simulations the feasible area of skyrmion nucle-

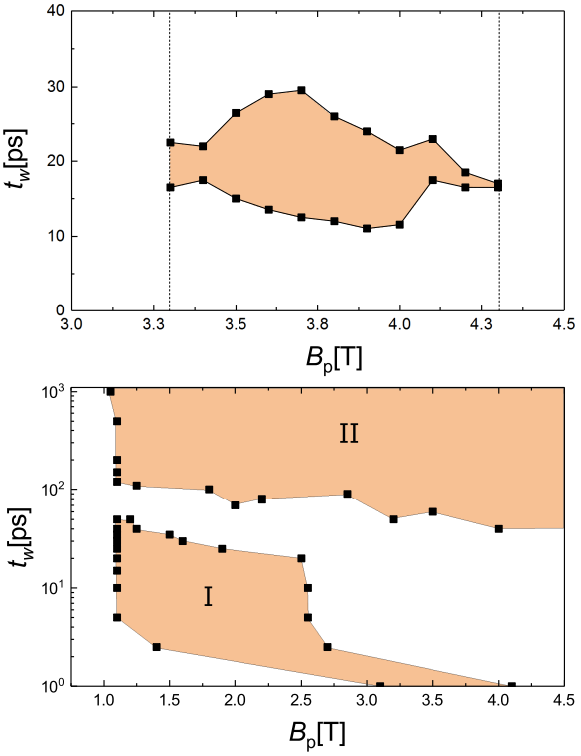

FIG. 4: (Color online) Phase diagram for the skyrmion nucleation induced by a magnetic field pulse: a) Atomistic simulation of single skyrmion generation by applying a uniform and perpendicular $\theta = 0$ magnetic field on a nanodisc with a size of $100a \times 3a$. Two vertical dashed lines indicate the minimum and maximum values of B_p for the nucleation of a skyrmion. b) Micromagnetic simulation of single (multiple) skyrmion generation, region I (II), by applying a localized and tilted magnetic field $\theta = 45^\circ$ to a CoPt disc of 500 nm.

ation by applying a uniform and perpendicular magnetic field is given by a pulse strength from 3.3 T to 4.3 T and a pulse width from 10 ps to 30 ps for the circular shaped system, Fig. 4 a. This phase diagram is material parameter dependent. To uncover whether this effect is only an edge effect, we did micromagnetic simulations for larger sample sizes in the presence of a localized and tilted applied magnetic field with a temporal and spatial Gaussian profile. Skyrmion nucleation is even observed in larger samples by applying spatially localized magnetic field pules either far from or close to the sample edges. Because the ground state is collinear, to excite high enough spin wave amplitudes one needs to apply a tilted magnetic field pulse in such large systems. In Fig. 4b the phase diagram of skyrmion nucleations for a CoPt nanodisc with diameter of 500 nm is plotted. The applied magnetic field is tilted 45°, with a Gaussian width of 100 nm. We checked the skyrmion nucleation for two different material parameters CoPt and FeGe thin films, see Supplemental Material [48]. FeGe has bulk DMI while CoPt has interfacial DMI and consequently these two different symmetries lead to two different skyrmion structures, namely hedgehog (Néel type) skyrmions and chiral vortex-like (Bloch type) skyrmions, respectively. In both samples we found two nucleation regimes depending on the magnetic field duration. Short pulses create single skyrmions, indicated as regime I in Fig. 4b, while longer pulses generate multiple skyrmions, indicated as regime II. Between these two regimes there is a gap in the phase space at which we could not find any stable skyrmion nucleation.

These numerical results can be easily understood by the following model. To overcome the barrier between a stable uniform ferromagnetic phase and a metastable skyrmionic phase, the ground state must be destabilized [44]. This is achieved by the creation of spin waves via the magnetic field pulse. Recently, it was shown that spin waves exert a torque on a uniform ferromagnet in the presence of both bulk and interfacial DMI [42]. Considering a uniform ferromagnetic state in which the DMI is smaller than a certain threshold, the magnonic spin-orbit torques are given by [42, 43],

$$\boldsymbol{T}^{\mathrm{SOT}} = \tau_{\parallel}\boldsymbol{m} \times (\hat{z} \times \boldsymbol{j}_m) + \tau_{\perp}\boldsymbol{m} \times (\hat{z} \times \boldsymbol{j}_m) \times \boldsymbol{m}, \quad (3)$$

where $\boldsymbol{j}_m = aJ\boldsymbol{m} \times \nabla\boldsymbol{m}$ is the spin wave current, and $\tau_{\parallel}$ and $\tau_{\perp}$ are phenomenological constants related to the DMI strength. We consider spin waves with frequency Ω and wavevector $\boldsymbol{k}$, as a deviation from a collinear state $\boldsymbol{m} = \hat{z} + \delta\boldsymbol{m}e^{i\Omega t + i\boldsymbol{k}\cdot\boldsymbol{r}}$. For simplicity we consider the surface anisotropy to be zero then,

$$\Omega = \frac{1 - i\alpha}{1 + \alpha^2}[a^2Jk^2 + \mu_s B_p + K + aJ(\tau_{\parallel} + i\tau_{\perp})(k_x + k_y)]. \quad (4)$$

By finding the external field in which the imaginary part of the dispersion relation becomes zero, $\mathrm{Im}[\Omega_{k,B_a^c}] = 0$, and minimizing it with respect to the wavevector, we find a nonzero critical wavevector $k_x^c = k_y^c = -(\tau_{\parallel} - \tau_{\perp}/\alpha)/(2a)$, that gives rise to the structural instability. Finally the critical field is given by,

$$\mu_s B_p^c = \frac{J}{2}(\tau_{\parallel} - \frac{\tau_{\perp}}{\alpha})^2 - K. \quad (5)$$

Eq. (5) shows the magnetic field required to generate spin waves with a given wavevector. The minimum magnetic field does not occur at the uniform mode $\boldsymbol{k} = 0$ as for ordinary spin wave excitations, but rather a spin wave with finite wavevector ($k_x = k_y \neq 0$) is excited by the magnetic field pulse. If $B_p > B_p^c$ then the system becomes destabilized.

The skyrmionic state in our simulations cannot be stabilized in the absence of DMI. This process occurs for a certain range of material parameters [47], e.g., the range of DMI, when $K/J \sim 0.1$, should be about $0.13 \leq D/J \leq 0.18$ in the atomistic trilayer circular sample. As the skyrmion diameter is proportional to $(D/J)^{-1}$, the skyrmion size is also limited. This range

of DMI strength is experimentally accessible [13, 45, 46]. Moreover, the damping value α is also important to create a skyrmion. We used here $\alpha = 0.05$, for both atomistic and micromagnetic simulations, which is a realistic value. For much higher damping than 0.05, the nucleation of a skyrmion cannot be stabilized due to the lack of sufficient spin wave propagation. This is in contrast with the current-induced single skyrmion case in which larger damping $\alpha > 0.1$, is needed [30]. Finally, within the parameter chosen in the case of a uniform magnetic field normal to the sample, the typical range of the amplitude of a pulse is 3 T to 4 T, with about 20 ps pulse width to nucleate an isolated skyrmion in the center of the nanodisc. On the other hand, in the case of applying a localized and tilted magnetic field, the threshold field amplitude is reduced to 0.5 T while the temporal field duration can be much longer. In general a large enough external perturbation is needed to trigger the instability of the uniform state.

In summary, we showed that in the presence of either bulk or interfacial DMI and in a specific range of realistic material parameters, skyrmions can be generated by means of a magnetic field pulse of picosecond duration. Both spatially uniform and non-uniform localized pulses can create skyrmions in small and large samples. To achieve such magnetic field amplitudes and durations one can also use the inverse Faraday effect arising from a circularly polarized laser pulse [49]. This method is faster than other methods which have been proposed yet and might be even used for skyrmion nucleation in ferromagnetic insulators as well as conducting ferromagnets. Our results may boost the building of a next-generation of magnetic devices utilizing the skyrmion state. Recently, it was shown that by using the interlayer exchange coupling, skyrmions can be stabilized in wider range of parameters [50]. Thus we expect generation of skyrmions by using magnetic field pulse might be applicable to a large class of materials.

Acknowledgments

Authors thank N. S. Kiselev, R. A. Duine, B. Dupe, M. V. Mostovoy and A. N. Bogdanov for fruitful discussions. This work was supported by the European union seventh framework program FP7-NMP-2011-SMALL-281043 (FEMTOSPIN), ERC grant agreement No. 339813 (EXCHANGE), and the Dutch science foundation NWO-FOM 13PR3118.

* Electronic address: alireza.qaiumzadeh@ntnu.no

[1] A. N. Bogdanov and D. A. Yablonskii, Sov. Phys. JETP. **68**, 101 (1989).
[2] A. Bogdanov and A. Hubert, J. Magn. Magn. Mater. **138**, 255 (1994).
[3] A. Bogdanov and A. Hubert, Phys. Status Solidi (b) **186**, 527 (1994).
[4] A. Bogdanov and A. Hubert, J. Magn. Magn. Mater. **195**, 182 (1999).
[5] U. K. Rößler, A. N. Bogdanov and C. Pleiderer, Nature. **442**, 797 (2006).
[6] U. K. Rößler, A. A. Leonov and A. N. Bogdanov, J. Phys. Conf. Ser. **303**, 012105 (2011).
[7] N. S. Kiselev, A. N. Bogdanov, R. Schäfer, and U. K. Rößler, J. Phys. D: Appl. Phys. **44**, 392001 (2013).
[8] A. Fert, V. Cros and J. Sampaio, Nat. Nanotechnol. **8**, 152 (2013).
[9] N. Nagaosa and Y. Tokura, Nat. Nanotechnol. **8**, 899 (2013).
[10] R. Tomasello, E. Martinez, R. Zivieri, L. Torres, M. Carpentieri, and G. Finocchio, Sci. Rep. **4**, 6784 (2014).
[11] J. Hagemeister, N. Romming, K. von Bergmann, E.Y. Vedmedenko, and R. Wiesendanger, Nat. Commun. **6**, 8455 (2015).
[12] X.C. Zhang, Y. Zhou, M. Ezawa, G. P. Zhao and W.S. Zhao, Sci. Rep. **5**, 11369 (2015).
[13] N. Romming, A. Kubetzka, C. Hanneken, K. von Bergmann, and R. Wiesendanger, Phys. Rev. Lett. **114**, 177203 (2015).
[14] M. Ezawa, Phys. Rev. Lett. **105**, 197202 (2010).
[15] N. S. Kiselev, A. N. Bogdanov, R. Schäfer, and U. K. Rößler, Phys. Rev. Lett. **107**, 179701 (2011).
[16] F. Büttner, C. Moutafis, M. Schneider, B. Krüger, C. M. Günther, J. Geilhufe, C. v. K. Schmising, J. Mohanty, B. Pfau, S. Schaffert, A. Bisig, M. Foerster, T. Schulz, C. A. F. Vaz, J. H. Franken, H. J. M. Swagten, M. Kläui, and S. Eisebitt, Nat. Phys. **11**, 225 (2015).
[17] S. Mühlbauer, B. Binz, F. Jonietz, C. Pfleiderer, A. Rosch, A. Neubauer, R. Georgii, and P. Boni, Science **323**, 915 (2009).
[18] X. Z. Yu, Y. Onose, N. Kanazawa, J. H. Park, J. H. Han, Y. Matsui, N. Nagaosa, and Y. Tokura, Nature **465**, 901 (2010).
[19] S. Heinze, K. von Bergmann, M. Menzel, J. Brede, A. Kubetzka, R. Wiesendanger, G. Bihlmayer and S. Blügel, Nat. Phys. **9**, 713 (2011).
[20] M. C. Langner, S. Roy, S. K. Mishra, J. C. T. Lee, X. W. Shi, M. A. Hossain, Y. D. Chuang, S. Seki, Y. Tokura, S. D. Kevan and R. W. Schoenlein, Phys. Rev. Lett. **112**, 167202 (2014).
[21] A. Mehlin, F. Xue, D. Liang, H. F. Du, M. J. Stolt, S. Jin, M. L. Tian, and M. Poggio, Nano Lett. **15**, 7, 4839 (2015).
[22] A. Dussaux, P. Schoenherr, K. Chang, N. Kanazawa, Y. Tokura, C. L. Degen and D. Meier, Nat. Commun. **7**, 12430 (2016).
[23] Y. Tokunaga, X. Z. Yu, J. S. White, H. M. Rnnow, D. Morikawa, Y. Taguchi, and Y. Tokura, Nat. Commun. **6**, 7638 (2015).
[24] S. Woo, K. Litzius, B. Krüger, M. Y. Im, L. Caretta, K. Richter, M. Mann, A. Krone, R. Reeve, M. Weigand, P. Agrawal, P. Fischer, M. Kläui and G. S. D. Beach, Nat. Mater. **15**, 501 (2016).
[25] C. Moreau-Luchaire, C. Moutafis, N. Reyren, J. Sampaio, N. Van Horne, C. A. F. Vaz, K. Bouzehouane, K. Garcia, C. Deranlot, P. Warnicke, P. Wohlhüter, J. M. George, J. Raabe, V. Cros and A. Fert, Nat. Nano. **11**, 444 (2016).

[26] A. Schlenhoff, P. Lindner, J. Friedlein, S. Krause, R. Wiesendanger, M. Weinl, M. Schreck and M. Albrecht, ACS Nano **9**, 6, 5908 (2015).

[27] X. Zhang, M. Ezawa and Y. Zhou, Sci. Rep. **5**, 9400 (2015).

[28] Y. Zhou and M. Ezawa, Nat. Commun. **5**, 4652 (2014).

[29] Y. Tchoe and J. H. Han, Phys. Rev. B **85**, 174416 (2012).

[30] S. -Z. Lin, C. Reichhardt and A. Saxena, Appl. Phys. Lett. **102**, 222405 (2013).

[31] J. Sampaio, V. Cros, S. Rohart, A. Thiaville and A. Fert, Nat. Nanotechnol. **8**, 839 (2013).

[32] J. Iwasaki, M. Mochizuki and N. Nagaosa, Nat. Nanotechnol. **8**, 742 (2013).

[33] W. Koshibae and N. Nagaosa, Nat. Commun. **5**, 5148 (2014).

[34] Y. Liu, G. Yin, J. Zang, J. Shi, and R. K. Lake, Appl. Phys. Lett. **107**, 152411 (2015).

[35] N. Romming, M. Menzel, C. Hanneken, J. E. Bickel, B. Wolter, K. von Bergmann, A. Kubetzka and R. Wiesendanger, Science **341**, 636 (2013).

[36] M. Finazzi, M. Savoini, A. R. Khorsand, A. Tsukamoto, A. Itoh, L. Duò, A. Kirilyuk, Th. Rasing, and M. Ezawa, Phys. Rev. Lett. **110**, 177205 (2013).

[37] J.-H. Moon, S.-M. Seo, K.-J. Lee, K.-W. Kim, J. Ryu, H.-W. Lee, R. D. McMichael, and M. D. Stiles, Phys. Rev. B **88**, 184404 (2013).

[38] J. L. García-Palacios and F. J. Lázaro, Phys. Rev. B **58**, 14937 (1998).

[39] A. Vansteenkiste, J. Leliaert, M. Dvornik, M. Helsen, F. Garcia-Sanchez, and B. VanWaeyenberge, AIP Advances **4**, 107133 (2014).

[40] B. Berg and M. Lüscher, Nucl. Phys. B, **190**, 412 (1981).

[41] D. S. G. Bauer, P. Mavropoulos, S. Lounis and S. Blügel, J. Phys. Condens. Matter **23**, 394204 (2011).

[42] A. Manchon, P. B. Ndiaye, J. H. Moon, H. W. Lee and K. J. Lee, Phys. Rev. B **90**, 224403 (2014).

[43] A.Qaiumzadeh, R. A. Duine, and M. Titov, Phys. Rev. B **92**, 014402 (2015).

[44] J. Shibata, G. Tatara and H. Kohno, Phys. Rev. Lett. **94**, 076601 (2005).

[45] J. H. Yang, Z. L. Li, X. Z. Lu, M.-H. Whangbo, S.-H. Wei, X. G. Gong, and H. J. Xiang, Phys. Rev. Lett. **109**, 107203 (2012).

[46] H. T. Nembach, J. M. Shaw, M. Weiler, E. Jué, and T. J. Silva, Nat. Phys. **11**, 825 (2015).

[47] C. Heo, N. S. Kiselev, A. K. Nandy, S. Blügel, and Th. Rasing, Sci. Rep **6**, 27146 (2016).

[48] See Supplemental Material at [URL will be inserted by publisher] for the phase diagram of skyrmion nucleation in FeGe thin films by applying a tilted magnetic field pulse as well as CoPt bilayers by applying a perpendicular magnetic field pulse.

[49] A. Kirilyuk, A. V. Kimel, and Th. Rasing, Rev. Mod. Phys. **82**, 2731 (2010); A. Qaiumzadeh, G. E. W. Bauer, and A. Brataas Phys. Rev. B **88**, 064416 (2013); A. Qaiumzadeh, M. Titov, *ibid* **94**, 014425 (2015).

[50] A. K. Nandy, N. S. Kiselev, and S. Blügel, Phys. Rev. Lett. **116**, 177202 (2016).